

A Study of Two-Dimensional Array Transducers for Limited Diffraction Beams

Jian-yu Lu, *Member, IEEE* and James F. Greenleaf, *Fellow, IEEE*

Abstract—The newly developed limited diffraction beams such as the Bessel beams and X waves have a large depth of field and approximate depth-independent property. They have possible applications in medical imaging, color Doppler imaging, tissue characterization, and nondestructive evaluation of materials, and in other wave related physical branches such as electromagnetics and optics. However, limited diffraction beams are currently produced with an annular array transducer that has to be steered mechanically. In this paper, we study the feasibility of steering these beams with a two-dimensional array, and show that there will be almost no distortion of beams if the effective aperture reduction of the array is properly compensated so that the beams have a constant transverse profile as they are steered. In addition, methods for reducing the complexity of the electronic multiplexing of the array elements are proposed. We also investigate the influences of the interelement distance and the size of array elements on the sidelobes and grating lobes of limited diffraction beams as the beams are steered. They are similar to those previously reported for conventional beams.

I. INTRODUCTION

THE FIRST limited diffraction beam called the Bessel beam was discovered by Durnin in 1987 [1]. Later, families of new limited diffraction beams have been discovered [2]–[6]. Theoretically, limited diffraction beams are produced with an infinite aperture radiator and energy and would propagate to an infinite distance without spreading. In practice, although limited diffraction beams can only be approximately realized with a finite aperture, they have a large depth of field and approximate depth-independent property [7]. Because of these features, limited diffraction beams may have applications in medical imaging [8]–[17], real-time color Doppler imaging [18], tissue characterization [19], nondestructive evaluation of materials [20], and other wave related physical branches such as electromagnetics [21]–[26] and optics [1], [7], [27]–[35]. Further details of limited diffraction beams and their trade-offs among the beam parameters such as sidelobes, resolution, frame rate, central frequency, bandwidth, aperture, and depth of field can be found in a review paper by Lu *et al.* [36]. Another technique to produce beams of large depth of field is called Axicon [37]–[39]. Beams produced by the Axicon do not satisfy a propagation-invariant solution of the scalar wave equation even if it was produced by an infinite aperture and energy. The failure of the application of a large Axicon [40] (15

cm in diameter operated at 4 MHz) on clinic breast imaging might be caused by the phase aberration of tissues [41],[42]. A detailed comparison of Axicon to limited diffraction beams has been reported in [36].

One way to approximately produce rotary symmetric limited diffraction beams is to use an annular array transducer [3], [8]–[12]. The advantage of annular arrays is their relatively few elements (from a few to about a dozen in medical imaging), and thus can be driven with simple electric circuits. However, annular arrays can only be scanned [10], [11] or steered mechanically (with a wobbler) [8]. Although a mechanically scanned or steered transducer produces high quality beams (maintaining low sidelobes, grating lobes, and small beamwidth, etc.) at any steering angle if refraction at the interface between the coupling medium and the skin is controlled [43], [44], it has the following disadvantages: The imaging frame rate is limited by the inertia of the transducer and its motor system; it is difficult to maintain a constant steering or scanning speed over the entire sweeping area; the probe (consisting of a transducer and motor system) vibrates when it is operated; the probe is subject to mechanical wear; and it is difficult to start and stop the transducer to shoot a beam several times in each transducer position as is desired in real-time color Doppler imaging [18].

Electronic beam scanning or steering can avoid the above disadvantages although it may have new problems such as grating lobes as well as the effective aperture reduction of transducers. It can be performed with one- or 2-D array transducers by applying linear delays to the electric signals of array elements or simply multiplexing a group of elements in the scan direction. One-dimensional arrays arrange elements in a line. They are widely used in modern commercial scanners for medical diagnosis because of their relatively fewer number of elements [45]. However, it is rather difficult for 1-D arrays to scan or focus beams electronically in an elevation plane of the arrays (a plane which is perpendicular to the scan plane that is defined by the line of elements and the axis of the arrays). In contrast, 2-D arrays arrange elements in a plane and thus can scan and focus beams electronically in any plane. They have been studied for conventional beams in slice-thickness reduction, volumetric imaging, and phase-aberration correction [46]–[49]. Because limited diffraction beams have a 2-D transverse profile, it is possible to produce, scan or steer them with a 2-D array.

In this paper, we study the feasibility of scanning or steering electronically limited diffraction beams with a 2-D array. As beams are steered off the normal axis of arrays, the area

Manuscript received November 5, 1993; revised March 1, 1994; accepted April 28, 1994. This work was supported in part by the National Institutes of Health by Grants CA 43920 and CA 54212.

The authors are with the Biodynamics Research Unit, Department of Physiology and Biophysics, Mayo Clinic and Foundation, Rochester, MN 55905 USA.

IEEE Log Number 9403355.

of the effective aperture of the arrays (the projection of the array aperture on the plane that is perpendicular to the beams) is reduced in the scan direction. The area reduction has a significant impact on the production of limited diffraction beams with 2-D arrays. Therefore, it is important to study compensation of the reduction of the area of the effective aperture and to simplify the complex electronic multiplexing resulting from the aperture compensation. Furthermore, influences of the interelement distance and size of elements of the arrays on the sidelobes, grating lobes, and distortions of limited diffraction beams, as well as their relations to steering angles are investigated. For the purpose of comparison, a focused Gaussian beam¹ [50] is also produced with the same arrays.

In Section II, we describe the scanning and steering of limited diffraction beams with a 2-D array transducer. Formulas for computer simulations and results are reported in Section III. Discussion and conclusion will be given in Sections IV and V, respectively.

II. SCANNING OR STEERING LIMITED DIFFRACTION BEAMS WITH A TWO-DIMENSIONAL ARRAY TRANSDUCER

A. Theoretical Limited Diffraction Beams

Limited diffraction beams are special types of solutions to the isotropic/homogeneous scalar wave equations [51], [52]. By limited diffraction we mean that traveling with the beams in their propagation directions, one sees no change in the wave patterns. This implies that limited diffraction beams would propagate to an infinite distance without spreading provided that they were produced with an infinite aperture and energy. Two particular limited diffraction beams, the Bessel beams and X waves, are given by the formulas [1], [2], [53]

$$\Phi_{J_m}(\vec{r}, t) = J_m(\alpha r) e^{i(\beta z - \omega t + m\phi)} \quad (1)$$

and

$$\Phi_{XBB_m}(\vec{r}, t) = \frac{a_0 (r \sin \zeta)^m e^{im\phi}}{\sqrt{M}(\tau + \sqrt{M})^m}, \quad (2)$$

respectively. In (1) and (2), $\Phi_{J_m}(\cdot)$ and $\Phi_{XBB_m}(\cdot)$ represent acoustic pressure or velocity potential, m is a nonnegative integer, $J_m(\cdot)$ is the m th-order Bessel function of the first kind, α denotes a scaling factor, $\beta = \sqrt{k^2 - \alpha^2}$, in which $k = \omega/c$ is the wavenumber, $\omega = 2\pi f_0$ is the angular frequency and f_0 is the central frequency, c is the speed of sound in the medium, $\vec{r} = (r, \phi, z)$ represents a point in space, $r = \sqrt{x^2 + y^2}$ is the radial distance from the wave axis, $\phi = \tan^{-1}(y/x)$ is the azimuthal angle in a transverse plane of beams, z is the axial distance, and t is time. Furthermore, $M = (r \sin \zeta)^2 + \tau^2$, where $\tau = [a_0 - i(z \cos \zeta - ct)]$, a_0 is a constant that controls the decay of the high-frequency components of X waves, and ζ is the Axicon angle.

To produce a broad-band Bessel beam, an electric δ -pulse (where $\delta = \delta(t)$ is the Dirac-Delta function) can be applied

¹ We choose the focused Gaussian beam as a representative of conventional focused beams because of its well-behaved beam shapes in the space. Therefore, the results of the analysis obtained from one depth may be extended to others.

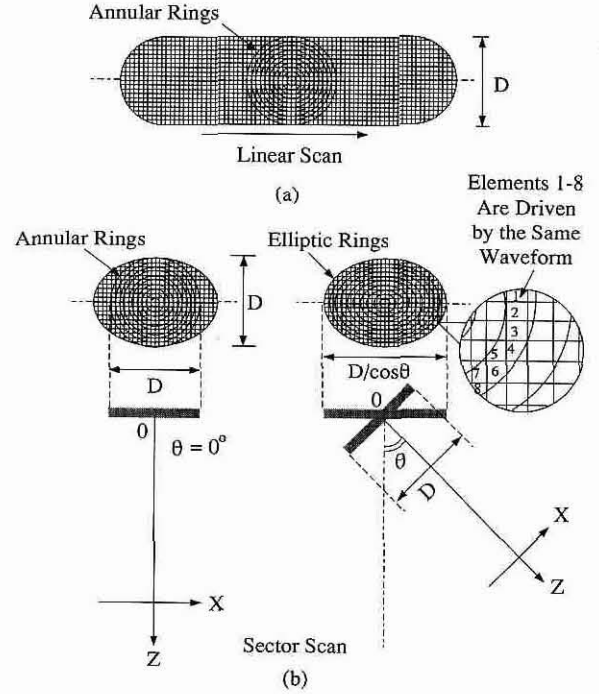


Fig. 1. Scanning or steering limited diffraction beams with a 2-D array transducer. The elements of the array are grouped into annular or elliptic rings. The same electrical drive signal is applied to each ring. (a) A 2-D array is used for a linear scan. (b) A 2-D array performs a sector scan by adding linear delays along the scan direction. The ring pattern is changed each time beams are steered to a new direction to compensate the effective aperture reduction of the array. (Modified with permission from Fig. 1 of [62]).

to drive the transducer. Suppose that the transmitting transfer function of the transducer is $B(\omega)$, the resulting Bessel pulses and X waves are given by [54]

$$\Phi_{JBL_m}(\vec{r}, t) = 2\pi e^{im\phi} J_m(\alpha r) \mathcal{F}^{-1}[B(\omega) e^{i\beta z}] \quad (3)$$

and

$$\Phi_{XBL_m}(\vec{r}, t) = \frac{1}{a_0} \mathcal{F}^{-1}[B(\omega)] * \Phi_{XBB_m}, \quad (4)$$

respectively, where “BL” stands for band-limited because the bandwidth of a practical transducer is always finite, \mathcal{F}^{-1} represents the inverse Fourier transform, and “*” represents convolution with respect to time.

B. Limited Diffraction Beams Produced with a Finite Aperture

In practice, limited diffraction beams can only be produced with a finite aperture transducer and thus have a finite depth of field. If the radius of the transducer is a , the depth of field of the Bessel beams and X waves are given by [1], [2]

$$BZ_{max} = a \sqrt{(k/\alpha)^2 - 1} \quad (5)$$

and

$$XZ_{max} = a \cot \zeta, \quad (6)$$

respectively.

The acoustic pressure or velocity potential of limited diffraction beams produced with a finite aperture transducer at any spatial point (field point), $\vec{r}_0 = (r_0, \phi_0, z)$ ($r_0 = \sqrt{x_0^2 + y_0^2}$

and $\phi_0 = \tan^{-1}(y_0/x_0)$, can be obtained with the Rayleigh-Sommerfeld diffraction formula [55]

$$\begin{aligned} \tilde{\Phi}(\vec{r}_0, \omega) = & \frac{1}{i\lambda} \int_0^a \int_{-\pi}^{\pi} \tilde{\Phi}(\vec{r}_1, \omega) e^{ikr_{01}} \frac{z}{r_{01}^2} r_1 dr_1 d\phi_1 \\ & + \frac{1}{2\pi} \int_0^a \int_{-\pi}^{\pi} \tilde{\Phi}(\vec{r}_1, \omega) e^{ikr_{01}} \frac{z}{r_{01}^3} r_1 dr_1 d\phi_1, \quad (7) \end{aligned}$$

where the first and second terms represent the high and low frequency contributions, respectively (in most applications, the second term is negligible), $\vec{r}_1 = (r_1, \phi_1, 0)$ ($r_1 = \sqrt{x_1^2 + y_1^2}$ and $\phi_1 = \tan^{-1}(y_1/x_1)$) is a point on the surface of the transducer (source point), λ is the wavelength, r_{01} is the distance between the field and source points, and $\tilde{\Phi}(\vec{r}_0, \omega)$ and $\tilde{\Phi}(\vec{r}_1, \omega)$ denote the temporal Fourier transform of the fields evaluated at the field and source points, respectively. For the Bessel beams and X waves, the weighting functions, $\tilde{\Phi}(\vec{r}_1, \omega)$, are the temporal Fourier transform of (3) and (4), respectively, evaluated at $z = 0$ [2]:

$$\tilde{\Phi}_{J_m}(\vec{r}_1, \omega) = 2\pi e^{im\phi_1} B(\omega) J_m(\alpha r_1) \quad (8)$$

and

$$\tilde{\Phi}_{X_m}(\vec{r}_1, \omega) = \frac{2\pi}{c} e^{im\phi_1} B(\omega) J_m(kr_1 \sin \zeta) H(\omega) e^{-k\alpha_0}, \quad (9)$$

where $H(\omega)$ is the Heaviside step function [56].

C. Producing Limited Diffraction Beams with an Annular Array Transducer

For $m = 0$, the zeroth-order limited diffraction beams in (1) and (2) or in (3) and (4) are rotary symmetric. Such rotary symmetric limited diffraction beams can be approximately produced with an annular array transducer [3], [10], [11]. Because an annular array transducer has only a finite number of elements, the aperture weighting functions given by (8) and (9) must be approximated with piecewise functions along the radial distance, i.e., $\tilde{\Phi}(\vec{r}_1, \omega) = \tilde{\Phi}(r_{1n}, \phi_1, \omega)$ if $r_{1n} \leq r_1 < r_{1(n+1)}$, where $n = 0, 1, 2, \dots, N-1$ and N is the number of elements. Note that for $N \rightarrow \infty$ and $\max(\Delta r_{1n}) \rightarrow 0$, where $\Delta r_{1n} = r_{1(n+1)} - r_{1n}$, the piecewise weighting functions are identical to the exact ones. In principle, the number of required elements depends on the spatial frequency of the weighting function along the radial distance. A higher spatial frequency requires a higher spatial sampling rate and thus a larger number of elements [57]. For a Bessel beam, three elements equally spaced in each lobe of the function, $|J_0(\alpha r_1)|$, are usually enough. An X wave that has the same -6 dB main beamwidth as the Bessel beam can also be produced with the same annular array with little distortion. As an example, a 14 element broadband annular array transducer has been used to produce a high resolution Bessel beam and X wave for real-time medical imaging [8]. The transducer has a diameter of 25 mm and central frequency of 3.5 MHz. The Bessel beam and X wave were produced with the following parameters: for the Bessel beam, $\alpha = 1217.51 \text{ m}^{-1}$, -6 dB lateral beamwidth is about 2.5 mm, and depth of field is about 150.0 mm in water; for the

X wave, $a_0 = 0.05$ mm, $\zeta = 4.75^\circ$, -6 -dB lateral beamwidth is also about 2.5 mm (depends on the central wavelength and Axicon angle of the X wave), and depth of field is about 150.43 mm. The positions of the 14 elements of the annular array are determined by $|J_0(\alpha r_1)|$ that has about 5 lobes. In each lobe, there are three equally spaced elements except the central lobe where there are two equally spaced elements. To produce the above Bessel beam and X wave, each element of the annular array is driven with a function calculated from (3) and (4), respectively, with $z = 0$ and $r_1 = r_{1n}$, where $n = 0, 1, 2, \dots, 13$. Consequently, a total of 14 transmitting waveforms or channels are required for the above annular array.

D. Scanning or Steering Limited Diffraction Beams

Although annular arrays can be used to produce limited diffraction beams with a small number of array elements, they can only be scanned or steered mechanically. The mechanical scanning or steering has the disadvantages such as low imaging frame rate, inconstant beam sweeping speed, probe vibration, mechanical wear, and causing artifacts in real-time color Doppler imaging [18]. Hence, it is desirable to scan or steer limited diffraction beams electronically. To perform electronic scanning or steering, 1- or 2-D arrays are employed. Because limited diffraction beams discovered thus far have a 2-D transverse profile, it is natural to use a 2-D array.

One way to scan or steer limited diffraction beams while still using the small number of drive waveforms is to group the elements of 2-D arrays into annular rings corresponding to annular arrays. To obtain a good approximation of annular arrays from 2-D arrays, the size of the elements must be smaller than the width of each annular ring. In addition, the number of elements must be large enough so that the interelement distance is small to ensure low grating lobes [46]. For the specific example of the above 14 element annular array, the average width of the ring is about 0.89 mm (2.08λ). In this case, the number of elements is determined mainly by the consideration of low grating lobes.

In medical imaging applications, several types of scans are available, such as, linear, curved linear², and sector scans. Here, we only discuss the linear and sector scans. The linear scan sweeps beams along a line without changing beam directions. The sector scan steers beams in a sector format with the apex of the sector fixed on or behind the center of the transducer surface. A scheme for the linear scan of limited diffraction beams is illustrated in Fig. 1(a), where an annular pattern is formed electronically by the elements of a 2-D array and is moved along the long axis of the array one element at a time. It is obvious that the farther the beams are swept, the larger the size of the array will be. For sector scan (beam steering), an annular pattern is also formed electronically by the array elements. However, beams are steered to a different direction by properly applying linear time delays to the signals of the elements in the scan direction. The number of elements required for the sector scan is usually smaller than that for the linear scan because the aperture for the sector scan is

²A curved linear scan is a variation of a linear scan and it employs the same mechanism to scan the beam as that in a linear scan.

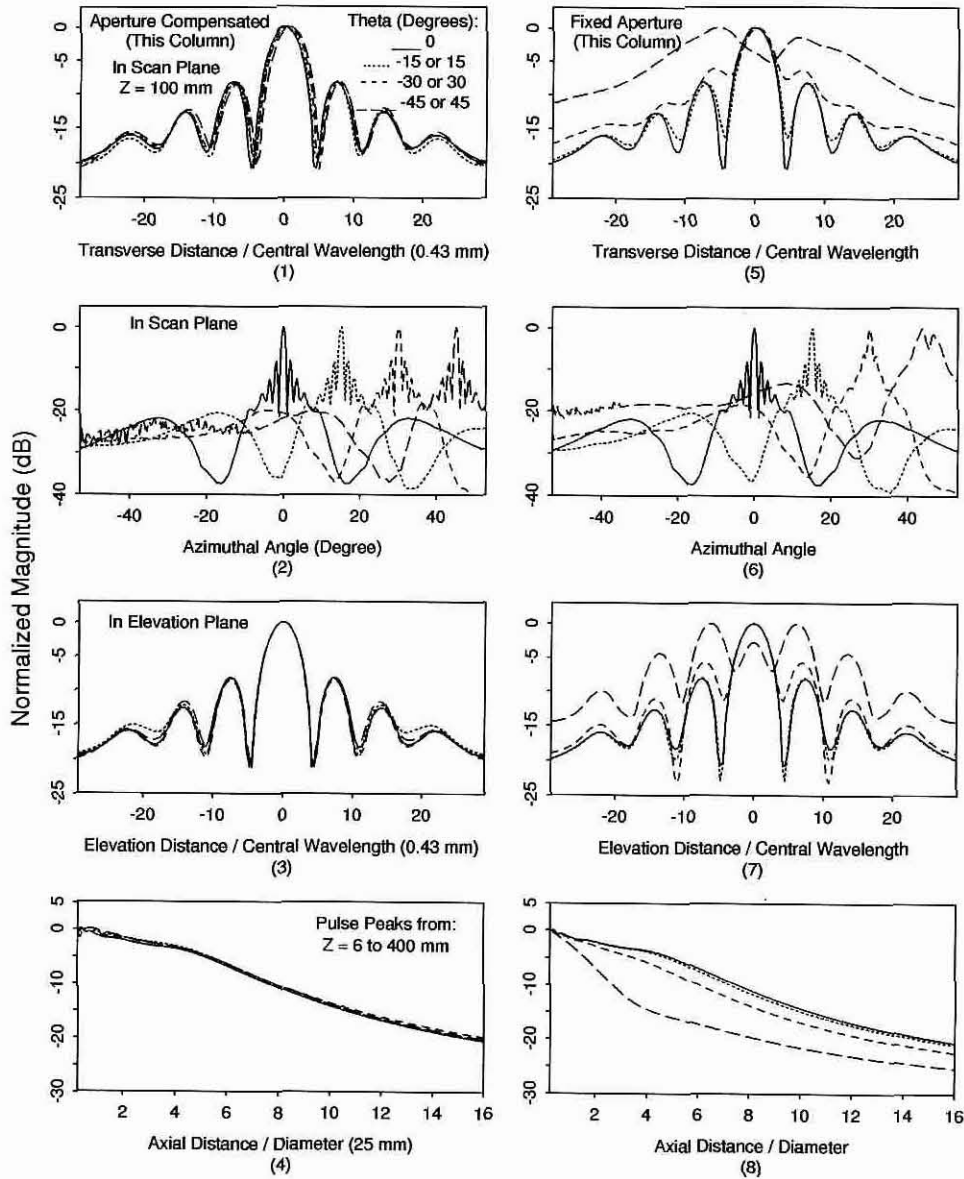


Fig. 2. Comparison of a one-way zeroth-order Bessel beam produced and steered with a 2-D array transducer with (panels in the left column) and without (panels in the right column) the compensation of the effective aperture reduction. The array is assumed to be composed of elements of infinite small size (point elements). The beam is steered at four angles: 0° (full lines), $\pm 15^\circ$ (dotted lines), $\pm 30^\circ$ (dashed lines), and $\pm 45^\circ$ (long dashed lines). The axial distance from the center of the array to the center of the Bessel pulse is 100 mm. The panels in the first row from the top are plots of the maxima of A-lines versus the axis (from -12.5 to 12.5 mm) that is perpendicular to the beam axis and in the scan plane (the plane defined by the beam axis and the scan direction). The panels in the second row from the top are plots of the maxima of A-lines in the arc strip defined by a radius from 87.5 mm to 112.5 mm from the array center versus the azimuthal angle from -53° to 53° in the scan plane. The panels in the third row from the top are plots of the maxima of A-lines versus an axis (from -12.5 to 12.5 mm) that is perpendicular to the scan plane (elevation direction). The panels in the bottom row are plots of the peaks of the Bessel pulses along the beam axis from 6 to 400 mm.

smaller [Fig. 1(b)]. Although a smaller aperture is used for the sector scan, the viewing areas are larger with deeper depth. The sector scan is especially useful where the size of acoustic windows are limited, e.g., in cardiac imaging. In this paper, we emphasize the sector scan scheme with a 2-D array transducer.

E. Compensation for Effective Aperture Reduction of Transducer

One of the disadvantages of electronic sector scanning is that the area of the effective aperture of arrays is reduced, as beams are steered off the array axis. This results in lower quality images in larger steering angles. This can be roughly

illustrated with human eyes that see clearer in a straight ahead direction and less clearly to the sides if the eyes and the head do not move. To compensate the effective aperture reduction, we suggest to use a varying aperture array that increases its aperture in the scan direction as beams steer so that the cross-section of the beams remains constant [Fig. 1(b)]. For the rotary symmetric limited diffraction beams, this implies that the annular pattern formed by the elements of a 2-D array is stretched into an elliptic pattern in the scan direction. The major axis of the elliptic pattern changes each time the beams are directed to a new position. In the next section, we will show the influence of the effective aperture reduction on the limited

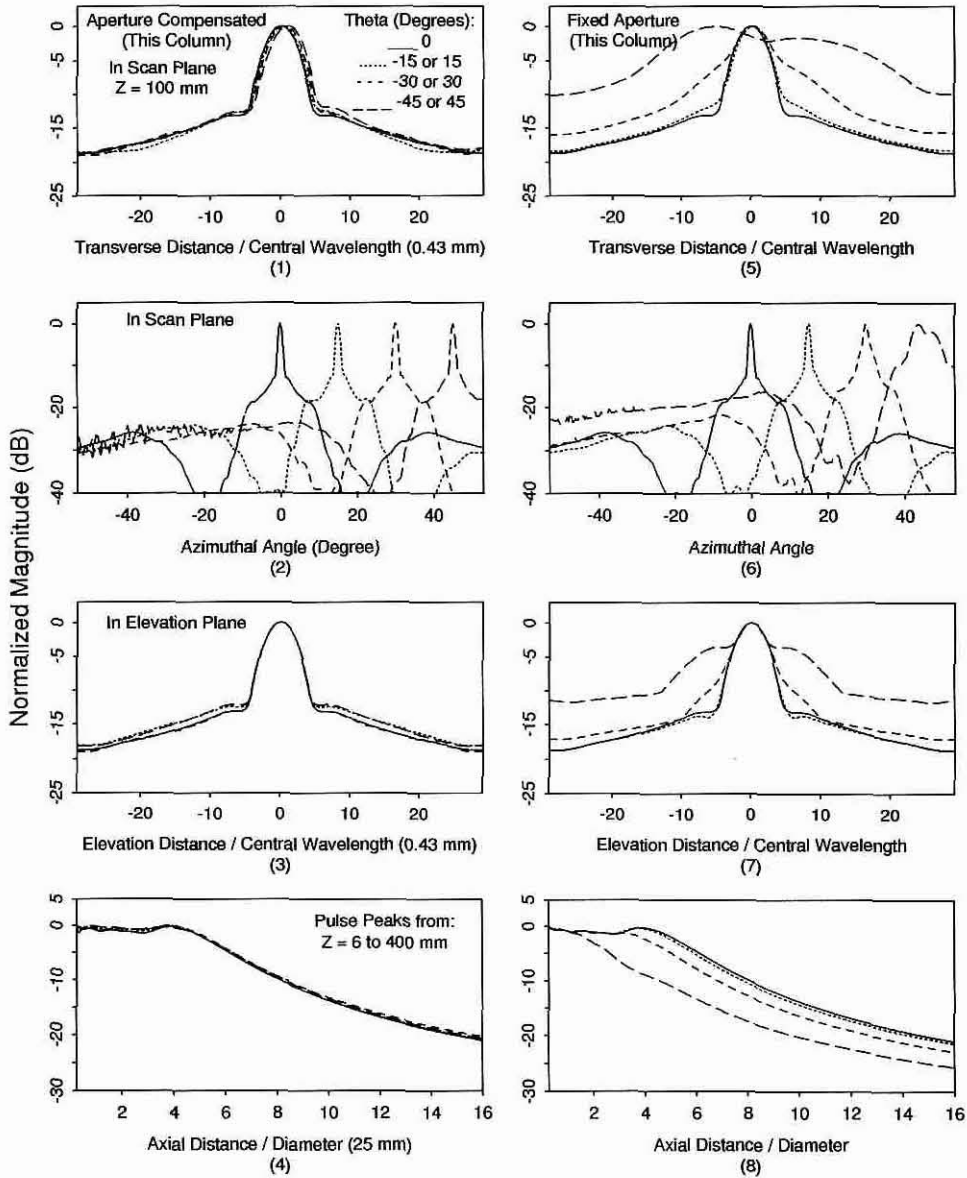


Fig. 3. Comparison of a one-way zeroth-order X wave produced and steered with a 2-D array transducer with (panels in left column) and without (panels in right column) the compensation of the effective aperture reduction. This figure has the same format and is obtained under the same array conditions as those of Fig. 2.

diffraction beams and the efficacy of the area compensation method.

III. SIMULATION AND RESULTS

A. Approximation and Quantization of Rayleigh-Sommerfeld Diffraction Formula

The Rayleigh-Sommerfeld diffraction formula (7) can be used to calculate fields of any aperture weightings. For a 2-D array, it can be rewritten as (neglect the second term and assume that the elements of the array are rectangular)

$$\tilde{\Phi}(x_0, y_0, z, \omega) = \frac{1}{i\lambda} \sum_{\mu} \sum_{\nu} \left\{ \tilde{\Phi}_{\mu\nu}(\omega) \int_{x_{1\mu}-w_{x_1}/2}^{x_{1\mu}+w_{x_1}/2} \int_{y_{1\nu}-w_{y_1}/2}^{y_{1\nu}+w_{y_1}/2} e^{ikr_{01}} \frac{z}{r_{01}^2} dx_1 dy_1 \right\}, \quad (10)$$

where $\sum_{\mu} \sum_{\nu}$ is a 2-D summation over all the elements of the array, w_{x_1} and w_{y_1} are widths of elements in the lateral (x_1) and vertical (y_1) directions on the transducer aperture, $(x_{1\mu}, y_{1\nu})$ denotes the coordinates of the center of the element in the ν th row and μ th column, and $\tilde{\Phi}_{\mu\nu}(\omega)$ is a stepwise weighting function that is equal to $\tilde{\Phi}(x_{1\mu}, y_{1\nu}, \omega)$ for the element centered at $(x_{1\mu}, y_{1\nu})$, and satisfies simultaneously the annular or elliptic ring constraint, i.e., $\tilde{\Phi}_{\mu\nu}(\omega) = \tilde{\Phi}(r_{1n}, \phi_1, \omega)$ when $r_{1n}/a \leq \sqrt{(x_{1\mu}/a_x)^2 + (y_{1\nu}/a)^2} < r_{1(n+1)}/a$, in which a_x and a are the major and minor axes of the elliptic rings (for annular rings, $a_x = a$). If a 2-D array is composed of point elements (point source elements), the above Rayleigh-Sommerfeld diffraction formula can be quantized

$$\tilde{\Phi}(x_0, y_0, z, \omega) \propto \frac{1}{i\lambda} \sum_{\mu} \sum_{\nu} \left\{ \tilde{\Phi}_{\mu\nu}(\omega) e^{ikr_{01\mu\nu}} \frac{z}{r_{01\mu\nu}^2} \right\}, \quad (11)$$

where $r_{01\mu\nu}$ is the distance between the point element at $(x_{1\mu}, y_{1\nu}, 0)$ and the field point at (x_0, y_0, z) , or

$$r_{01\mu\nu} = \sqrt{(x_{1\mu} - x_0)^2 + (y_{1\nu} - y_0)^2 + z^2}. \quad (12)$$

The Rayleigh-Sommerfeld diffraction formula in (10) contains double integrals and thus is time consuming in computation. With the Fresnel approximation [55], the double integrals can be simplified to two single ones. This is done as follows. The distance between the source and field points in (10) is given by

$$r_{01} = \sqrt{(x_1 - x_0)^2 + (y_1 - y_0)^2 + z^2}. \quad (13)$$

With the substitutions of variables, $x_1 = x_{1\mu} + \Delta x_1$ and $y_1 = y_{1\nu} + \Delta y_1$, the above source-field distance is simplified to

$$r_{01} \approx r_{01\mu\nu} + \frac{2\Delta x_1(x_{1\mu} - x_0) + 2\Delta y_1(y_{1\nu} - y_0) + (\Delta x_1)^2 + (\Delta y_1)^2}{2r_{01\mu\nu}}, \quad (14)$$

if the condition, $2\Delta x_1(x_{1\mu} - x_0) + 2\Delta y_1(y_{1\nu} - y_0) + (\Delta x_1)^2 + (\Delta y_1)^2 \ll r_{01\mu\nu}^2$, is satisfied. Substituting (14) into the phase term and replacing r_{01} with $r_{01\mu\nu}$ in the denominator of (10), one obtains the following

$$\begin{aligned} \tilde{\Phi}(x_0, y_0, z, \omega) = & \frac{z}{i\lambda} \sum_{\mu} \sum_{\nu} \frac{\tilde{\Phi}_{\mu\nu}(\omega)}{r_{01\mu\nu}^2} e^{ikr_{01\mu\nu}} \\ & \cdot \left[\int_{-w_{x_1}/2}^{w_{x_1}/2} e^{ik \frac{2\Delta x_1(x_{1\mu} - x_0) + (\Delta x_1)^2}{2r_{01\mu\nu}}} d\Delta x_1 \right] \\ & \cdot \left[\int_{-w_{y_1}/2}^{w_{y_1}/2} e^{ik \frac{2\Delta y_1(y_{1\nu} - y_0) + (\Delta y_1)^2}{2r_{01\mu\nu}}} d\Delta y_1 \right]. \end{aligned} \quad (15)$$

To steer beams in the lateral (x_1) direction, (10), (11), or (15) must be multiplied with a quantized linear phase term, $e^{-ikx_{1\mu} \sin \theta}$, inside the summations, where θ is the angle between the beam axis and the array axis. After obtaining the continuous wave (CW) fields from (10), (11), or (15), for all frequency components, broad-band beams can be obtained by the inverse Fourier transform.

B. Results

In the following, we will show influences of the effective aperture reduction on beams that are steered electronically with a 2-D array. We also show the effects of the interelement distance and size of elements on the sidelobes, grating lobes, and main beamwidth of limited diffraction beams and their relationships to the steering angles.

The zeroth-order Bessel beam and X wave that have the parameters as those in section II.C and are produced with a 2-D array consisting of point elements are shown in Figs. 2 and 3 (calculated with (11)), respectively. These beams are obtained at $z/D = 4.0$, where z and D denote the axial distance

(100 mm) and diameter (25 mm) of the array in the elevation direction (y_1 direction), respectively. The 2-D array has the same interelement distance (0.64 mm) in both the lateral (scan) and elevation directions, i.e., $d_{x_1} = d_{y_1} \approx 1.5\lambda$, and the elements of the array are grouped into 14 annular or elliptic rings depending on the steering angle and are driven by 14 waveforms. The drive waveforms for the Bessel beam and X wave are calculated from (3) and (4), respectively, with $z = 0$, $m = 0$, and $r = r_{1n}$, where r_{1n} ($n = 0, 1, \dots, 13$) are the central radii of the annular rings in the transverse plane of the beams (projected from the array aperture), or calculated from the spectra of these waveforms, (8) and (9), respectively. The transmitting transfer function of the transducer, $B(\omega)$, in (3) and (4), or in (8) and (9), is assumed to be a Blackman window function³ [57] peaked at $f_0 = 3.5$ MHz, with a relative bandwidth of about 81% (-6 dB one-way bandwidth divided by the central frequency). Figs. 2 and 3 show that the beams are distorted greatly if they are steered with a fixed aperture array (right columns). When steered with a variable aperture array that is properly compensated for the effective aperture reduction, the beams have almost no distortions (left columns). As a comparison, a focused Gaussian beam that is also produced with 14 drive waveforms (pulses with their amplitudes determined by a Gaussian function evaluated at r_{1n}) and with the same fixed-aperture or aperture-compensated 2-D arrays is shown in Fig. 4. The Gaussian beam has a lateral full-width-at-half-maximum (FWHM) beamwidth of about 12.5 mm (equal to the radius of the array in the elevation direction) at the surface of the transducer and a FWHM of about 3.03 mm in the focal plane (the focal length, F , is 100 mm, or the f -number, F/D , is 4.0). With a fixed aperture, the beamwidth of the focused Gaussian beam is greatly increased in the scan direction because of the effective aperture reduction and is almost unchanged in the elevation direction. This is different from the limited diffraction beams (Figs. 2 and 3) and indicates that the two orthogonal lateral directions of conventional beams are uncoupled. It also worth noting that the focal length is decreased as the steering angle is increased (Panel (4) of Fig. 4) due to the fact that the curvature of the wavefront in the scan direction is increased (assuming that focusing delays are fixed for the array elements).

Similar to the case of 2-D arrays for conventional beams [46], the interelement distance of the arrays also affects the grating lobes of limited diffraction beams. The magnitude of the grating lobes is increased and the distances between the grating lobes and mainlobes are decreased as the interelement distance of the arrays increases. This fact can be illustrated by Figs. 5 to 7 (calculated also from (11) by assuming that the arrays are composed of point elements and have been properly compensated for the effective aperture reduction) for the zeroth-order Bessel beam, X wave, and conventional focused Gaussian beam, respectively. In particular, with the interelement distance of 1.28 mm ($d_{x_1} = d_{y_1} \approx 3.0\lambda$), the grating lobes become so high and so close to the mainlobes that

³We have found that the simulations are very close to the experiment when a Blackman window function is used to model the transfer function of an actual resonant-type transducer [11]. Other window functions, such as the Gaussian function, should produce similar results.

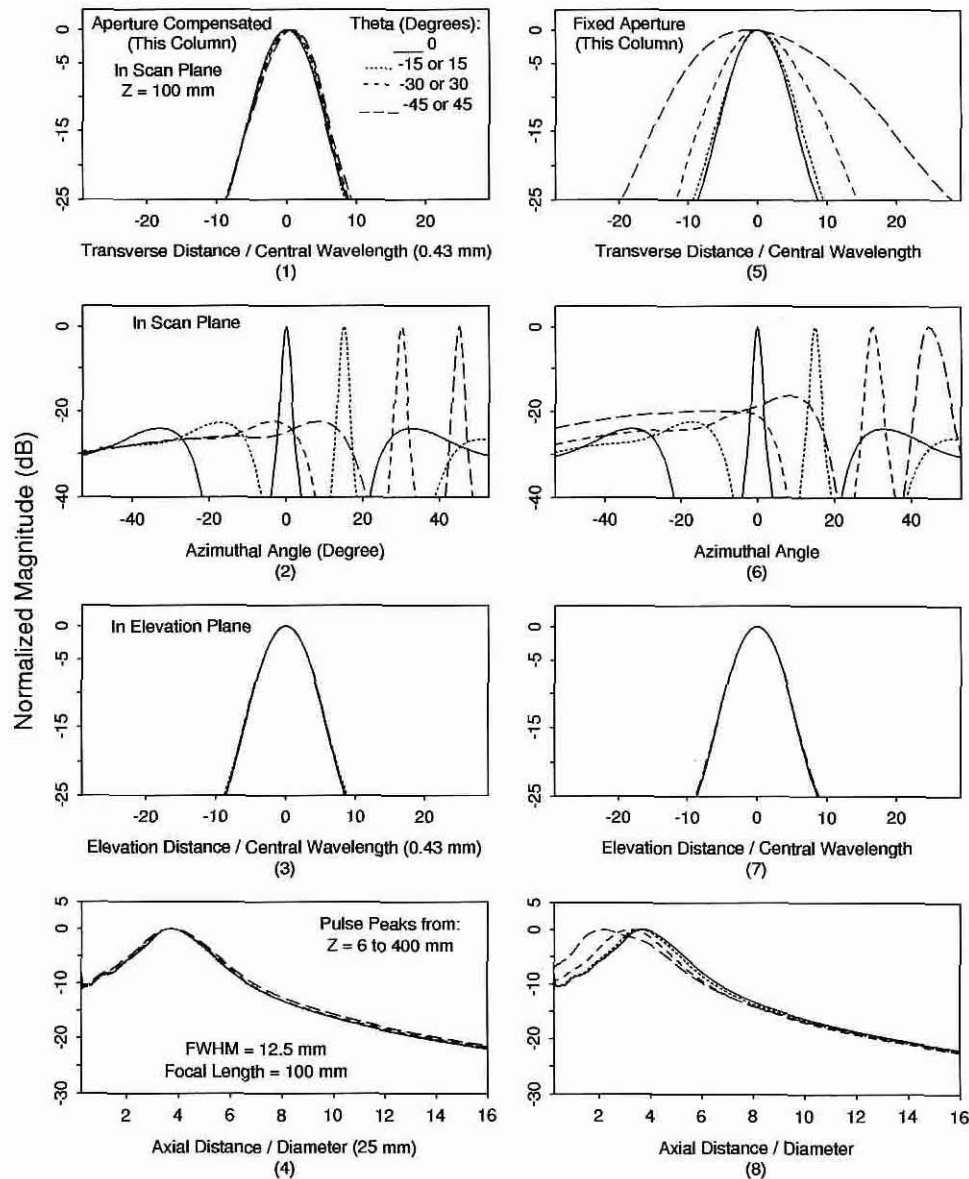


Fig. 4. Comparison of a one-way focused Gaussian beam (the focal length is 100 mm and the FWHM is 12.5 mm at the transducer aperture in the elevation direction) produced and steered with a 2-D array transducer with (panels in the left column) and without (panels in the right column) the compensation of the effective aperture reduction. This figure has the same format and is obtained under the same array conditions as those of Fig. 2.

they even increase the sidelobes. In this case, the interelement distance is even greater than the average distance between the annular rings (about 2.08λ) in the elevation direction. In contrast, when the interelement distance decreases to a certain value, say, 0.16 mm ($d_{x_1} = d_{y_1} \approx 0.37\lambda$), the grating lobes are moved so far away from the mainlobes that they cannot be seen from Figs. 5 to 7 (Panel (4)). Because the number of the elements of a 2-D array for a given aperture is inversely proportional to the square of the interelement distance, one must compromise between the number of elements and the grating lobes. In this paper, we choose the interelement distance to be 0.64 mm (about 1.5λ) to ensure that the magnitude of the one-way grating lobes are at least 20 dB below the peak of beams and the grating lobes are separated from the main lobes (Panel (2) of Figs. 5 to 7). For this specific interelement distance, the minimum required

number of array elements is about 1700 when steered from -45° to $+45^\circ$ with the compensation of the effective aperture reduction. (This number of elements may be further reduced as will be shown in the next section.) It is well known that the magnitude of the grating lobes of a CW driven array is about the same as that of the mainlobe [58]. However, the magnitude of the grating lobes in Figs. 5 to 7 are much lower than that of the mainlobes. This is because the beams in Figs. 5 to 7 are broadband, which will in general reduce the number of array elements contributing coherently to the grating lobes than to the mainlobes [45], [46].

In addition to the influence of the interelement distance, the size of array elements also has significant influence on the array performances. To illustrate this fact, we plot in Figs. 8 to 10, respectively, the zeroth-order Bessel beam, X wave, and focused Gaussian beam produced with a 2-D array of

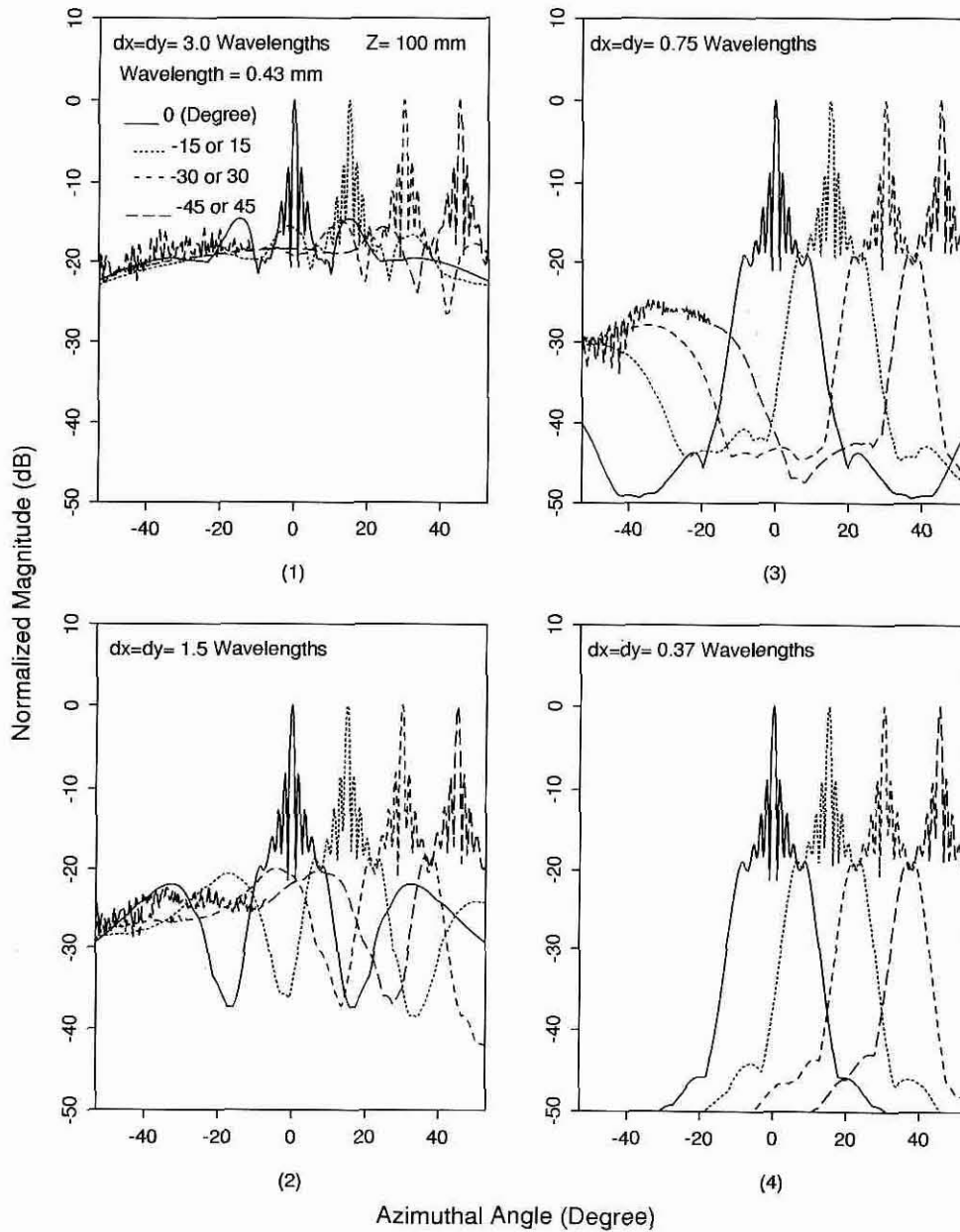


Fig. 5. Influence of interelement distances of a 2-D array on grating lobes of a one-way zeroth-order Bessel beam at four steering angles: 0° (full lines), $\pm 15^\circ$ (dotted lines), $\pm 30^\circ$ (dashed lines), and $\pm 45^\circ$ (long dashed lines). The array is assumed to be composed of elements of infinite small size (point elements). The interelement distances in both the scan and elevation directions are assumed to be the same, i.e., $d_{x_1} = d_{y_1}$. Four interelement distances are calculated for the beam: (1) 1.28 mm (about 3.0λ), (2) 0.64 mm (about 1.5λ), (3) 0.32 mm (about 0.75λ), and (4) 0.16 mm (about 0.37λ), where the central wavelength, λ , is about 0.43 mm. The axial distance from the center of the array to the center of the Bessel pulse is 100 mm. The figure shows the plots of the maxima of A-lines in the arc strip defined by a radius from 87.5 mm to 112.5 mm from the array center versus the azimuthal angle from -53° to 53° in the scan plane.

an interelement distance of about 1.5λ in both the scan and elevation directions ($d_{x_1} = d_{y_1} \approx 1.5\lambda$). The beam parameters used in Figs. 8 to 10 are the same as those for the left columns (with the compensation of the effective aperture reduction) of Figs. 2 to 5, except that the size (or width) of elements are taken into account (computed with (15)). The size of elements in the elevation direction in Figs. 8 to 10 is fixed ($w_{y_1} \approx 1.5\lambda$), and the elements have three sizes in the scan direction, i.e., w_{x_1} is about 0.37λ (left columns), 0.75λ (middle columns), and 1.5λ (right columns), respectively. As w_{x_1} increases, the grating lobes are reduced when the steering angle is small. However, for large w_{x_1} , the grating lobes, sidelobes, and the

beam width of the mainlobe are increased dramatically with the steering angle (Figs. 8 to 10). In addition, the magnitude of the peaks of the beams decreases much faster with the increase of the steering angle for a larger w_{x_1} (Table I). On the other hand, with a small w_{x_1} , say 0.37λ , the array performances are very close to those with an infinite small element width (point elements) (compare the left columns of Figs. 8 to 10 to those of Figs. 2 to 4, and see also Table I). The size of elements in the elevation direction, w_{y_1} , has little influence on the grating lobes of the beams except at $w_{x_1} = d_{x_1}$ and $w_{y_1} \rightarrow d_{y_1}$, where the grating lobes are reduced dramatically when the steering angle is small.

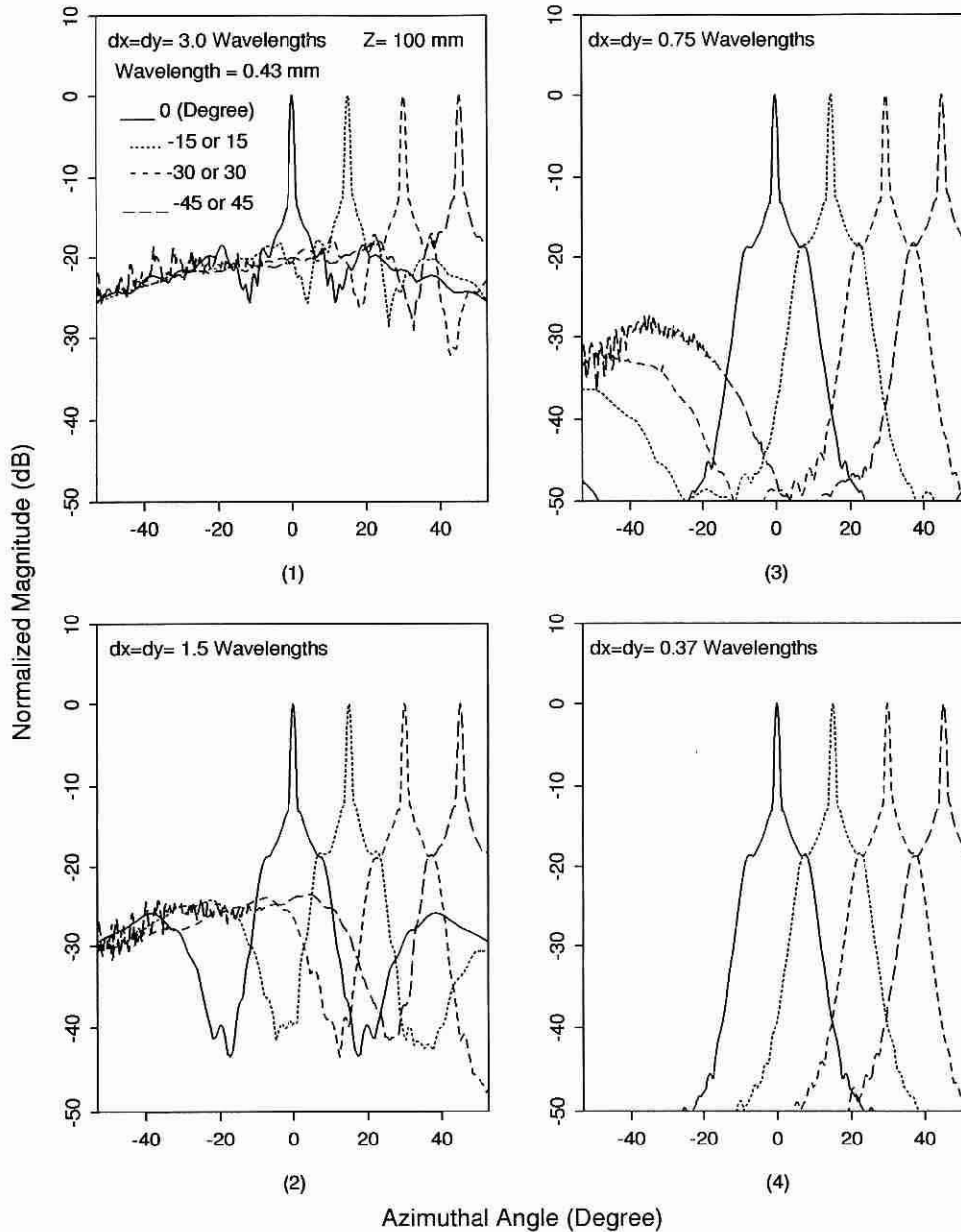


Fig. 6. Influence of interelement distances of a 2-D array on grating lobes of a one-way zeroth-order X wave at four steering angles: 0° (full lines), $\pm 15^\circ$ (dotted lines), $\pm 30^\circ$ (dashed lines), and $\pm 45^\circ$ (long dashed lines). This figure has the same format and is obtained under the same array conditions as those of Fig. 5.

The reason that the size of elements in the scan direction has a significant influence on grating lobes might be explained as follows. As the size of elements increases, the directivity pattern of each element becomes narrower and produces larger phase fluctuations in larger observation angles [46]. This can be seen from the first integration in (15), where the integrand,

$$e^{ik \frac{2\Delta x_1(x_{1\mu} - x_0) + (\Delta x_1)^2}{2r_{01\mu\nu}}} \approx e^{-ik \frac{\Delta x_1 x_{0c}}{z}}, \quad (16)$$

oscillates faster if Δx_1 changes over a larger element width (w_{x_1}) at a larger steering angle, $\theta = \tan^{-1} x_{0c}/z$, where x_{0c} is the coordinate of the beam center in the scan direction. This may cause a serious phase cancellation in (15). However, as the size of elements reduces, the impedance of elements will be increased, which makes impedance matching difficult. In

addition, if the size of elements is reduced and the number of elements is not increased accordingly, the energy efficiency of an array is decreased because only a part of the array aperture is used. Hence, one has to compromise between the size of elements and the array performance. From Figs. 8 to 10, one may wish to choose $w_{x_1} = d_{x_1}/2 \approx 0.75\lambda$ and $w_{y_1} = d_{y_1} \approx 1.5\lambda$ for an optimal performance.

IV. DISCUSSION

A. Sidelobes and Grating Lobes of Limited Diffraction Beams

We have demonstrated in the previous sections that compensation for the effective aperture reduction of a 2-D array so that the transverse cross section of a beam remains constant for all steering angles is essential for a proper production of

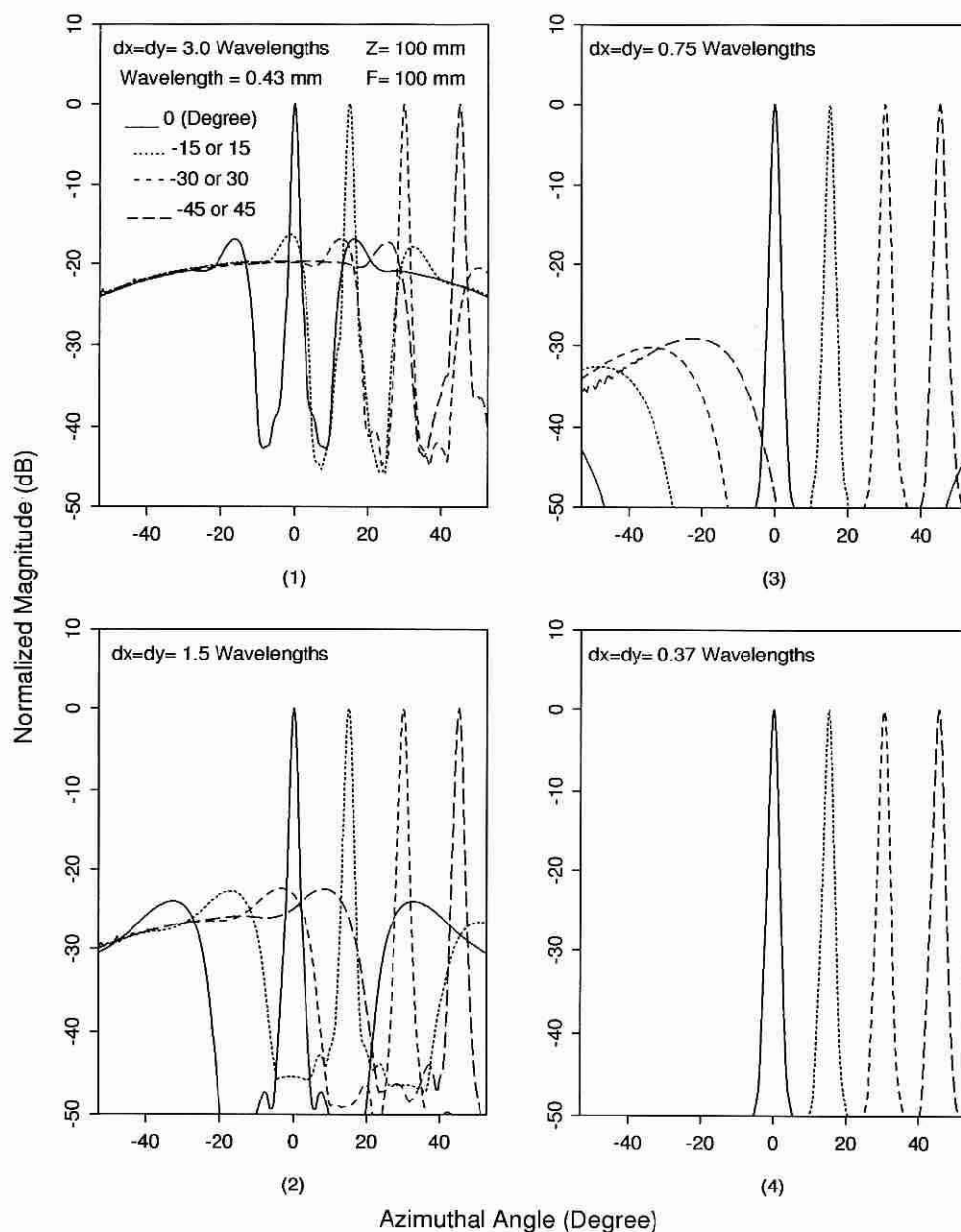


Fig. 7. Influence of interelement distances of a 2-D array on grating lobes of a one-way focused Gaussian beam (the focal length is 100 mm and the FWHM is 12.5 mm at the transducer aperture in the elevation direction) at four steering angles: 0° (full lines), ±15° (dotted lines), ±30° (dashed lines), and ±45° (long dashed lines). This figure has the same format and is obtained under the same array conditions as those of Fig. 5.

limited diffraction beams (Figs. 2 and 3). Without the proper compensation, sidelobes, grating lobes and lateral width of beams will be increased as the beams are steered away from the normal direction of the array. At larger steering angles, the mainlobes of the beams may even disappear because the sidelobes exceed them. An uncompensated array also produces beams that are distorted in both the scan and elevation directions and a reduced depth of field (Figs. 2 and 3). In addition, as we have seen from Fig. 4, the beamwidth of conventional focused beams is increased in the scan direction because of the effective aperture reduction in this direction. The focal length is shortened because the curvature of the wavefront increases with the decrease of the effective aperture if time delays for focusing are fixed for elements. However, unlike limited diffraction beams, distortions caused by the effective aperture

reduction are not coupled in the two transverse orthogonal directions of conventional beams.

Even with the proper compensation of the effective aperture reduction, the sidelobes of limited diffraction beams are still high (determined by (1) or (2)) as compared to those of conventional focused beams at their focuses (Figs. 2 to 4). The sidelobes of limited diffraction beams can be reduced by a summation-subtraction method [54], [59], deconvolution [9], [60], [61], and dynamically focused reception [8], [43], [44]. Grating lobes are about the same for both limited diffraction beams and conventional beams and are mainly determined by the interelement distance of arrays (Figs. 5 to 7). Broadband arrays may help to reduce the grating lobes. If the size of array elements is infinitely small (point elements, (Panel (2) of Figs. 2 to 4, and Figs. 5 to 7)), grating lobes are

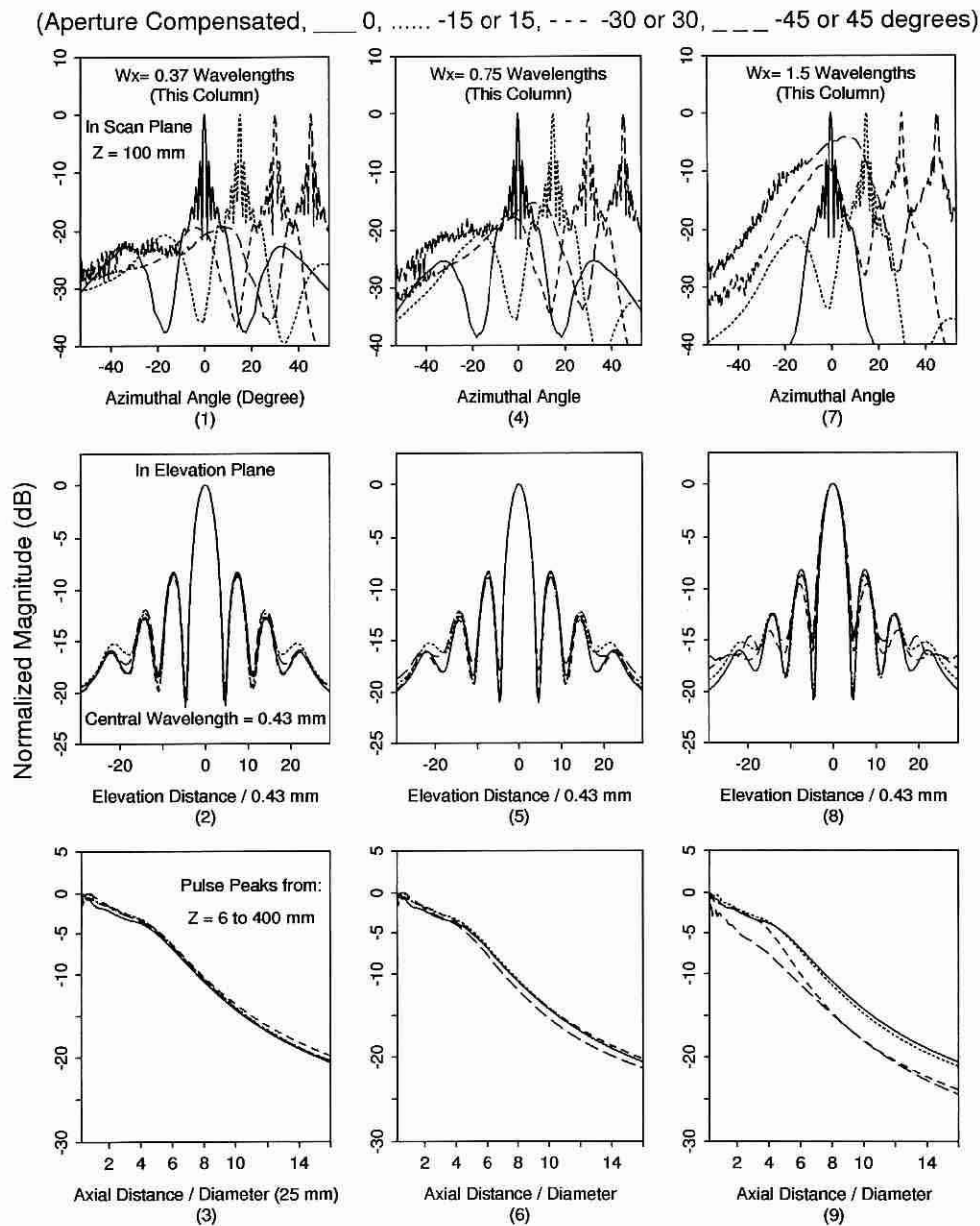


Fig. 8. Comparison of a one-way zeroth-order Bessel beam produced with a 2-D array transducer when the widths of the array elements in the scan direction are about 0.37λ (panels in the left column), 0.75λ (panels in the middle column), and 1.5λ (panels in the right column). The width of the array elements in the elevation direction is fixed to be about 1.5λ . The interelement distances in both the scan and elevation directions are the same and are also about 1.5λ . The beam is steered at four angles: 0° (full lines), $\pm 15^\circ$ (dotted lines), $\pm 30^\circ$ (dashed lines), and $\pm 45^\circ$ (long dashed lines). The axial distance from the center of the array to the center of the Bessel pulse is 100 mm. The panels in the first row from the top are plots of the maxima of A-lines in the arc strip defined by a radius from 87.5 mm to 112.5 mm from the array center versus the azimuthal angle from -53° to 53° in the scan plane. The panels in the middle row are plots of the maxima of A-lines versus an axis (from -12.5 to 12.5 mm) that is perpendicular to the beam axis and in the scan plane. The panels in the bottom row are plots of the peaks of the Bessel pulses along the beam axis from 6 to 400 mm.

almost independent of the steering angles. As the size of elements increases in the scan direction, array performance parameters (grating lobes, sidelobes, main beamwidth, and gain) are degraded dramatically at large steering angles.

B. Reducing Number of Elements

It is also clear from the previous sections that to reduce grating lobes or to produce limited diffraction beams of a high lateral resolution, the interelement distance of a 2-D array must be small [46]. However, a small interelement distance means a large number of elements for an array with a given aperture.

Therefore, there is a trade-off between the grating lobes and the number of elements. For example, if the interelement distance is about 1.5λ in both the scan and elevation directions, the number of elements of an elliptic array (for the purpose of compensating the effective aperture reduction) with its major and minor axes of about 17.7 mm (about 41.2λ) and 12.5 mm (about 29.2λ), respectively, is about 1700. The interelement distance may be even smaller if the grating lobes are required to be much lower than -20 dB (Figs. 5 to 7). The large number of elements of a 2-D array in a small aperture may cause problems such as difficulty in wiring, electronic and

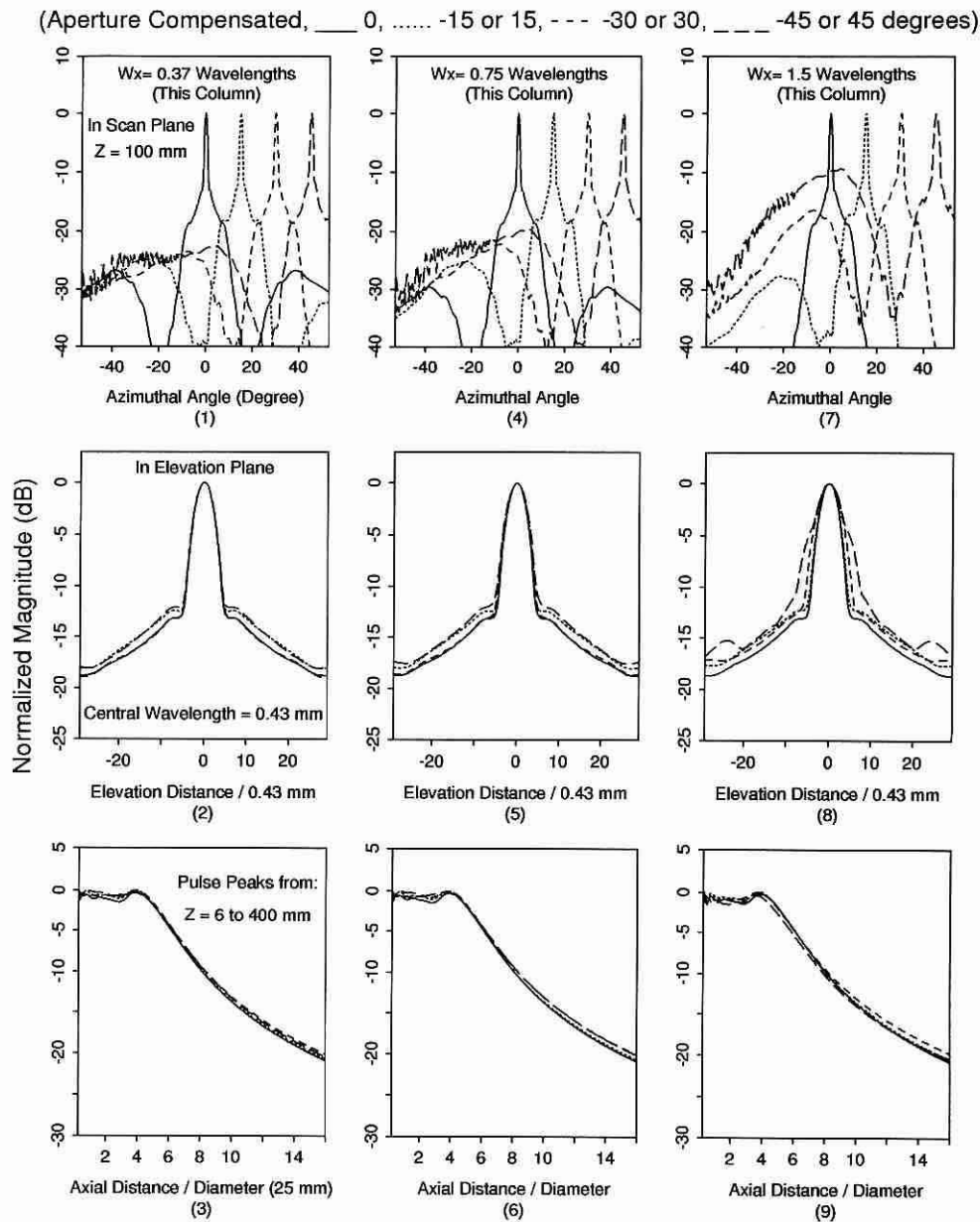


Fig. 9. Comparison of a one-way zeroth-order X wave produced with a 2-D array transducer when the widths of the array elements in the scan direction are about 0.37λ (panels in the left column), 0.75λ (panels in the middle column), and 1.5λ (panels in the right column). This figure has the same format and is obtained under the same array conditions as those of Fig. 8.

mechanical crosstalk among elements, high impedance of each element, and complex multiplexing among elements [46].

Some techniques have been suggested to reduce the number of elements of 2-D arrays while maintaining a reasonably good array performance. Sparse arrays, for example, reduce the number of elements by randomly removing elements from periodic dense arrays. However, array performance suffers because of increased sidelobes and loss of gain [46]. Another way to form a space array is to place randomly a fewer number of elements within the array aperture (random position array). This increases the randomness of the array and is expected to reduce grating lobes, but such arrays may be difficult to construct. In addition, the distance between some of the elements may be small, which limits the size of these elements and increases further their impedance. To avoid the small

interelement distances, one may limit the distance between the centers of any two elements to be greater than a given value. But, as the minimum interelement distance increases, there will be more restrictions on element positioning which will reduce the array randomness.

C. Size of Elements

A larger element size in the scan direction has a significant influence on the performances of a 2-D array at larger steering angles (Figs. 8 to 10, and Table I). On the other hand, a small element size increases the impedance of the elements and makes impedance matching difficult, resulting in low sensitivity, high noise, and high cross-talk, although a multilayer 2-D array technique [63] may be used to increase the impedance to some extent. Wiring is also difficult for the small elements

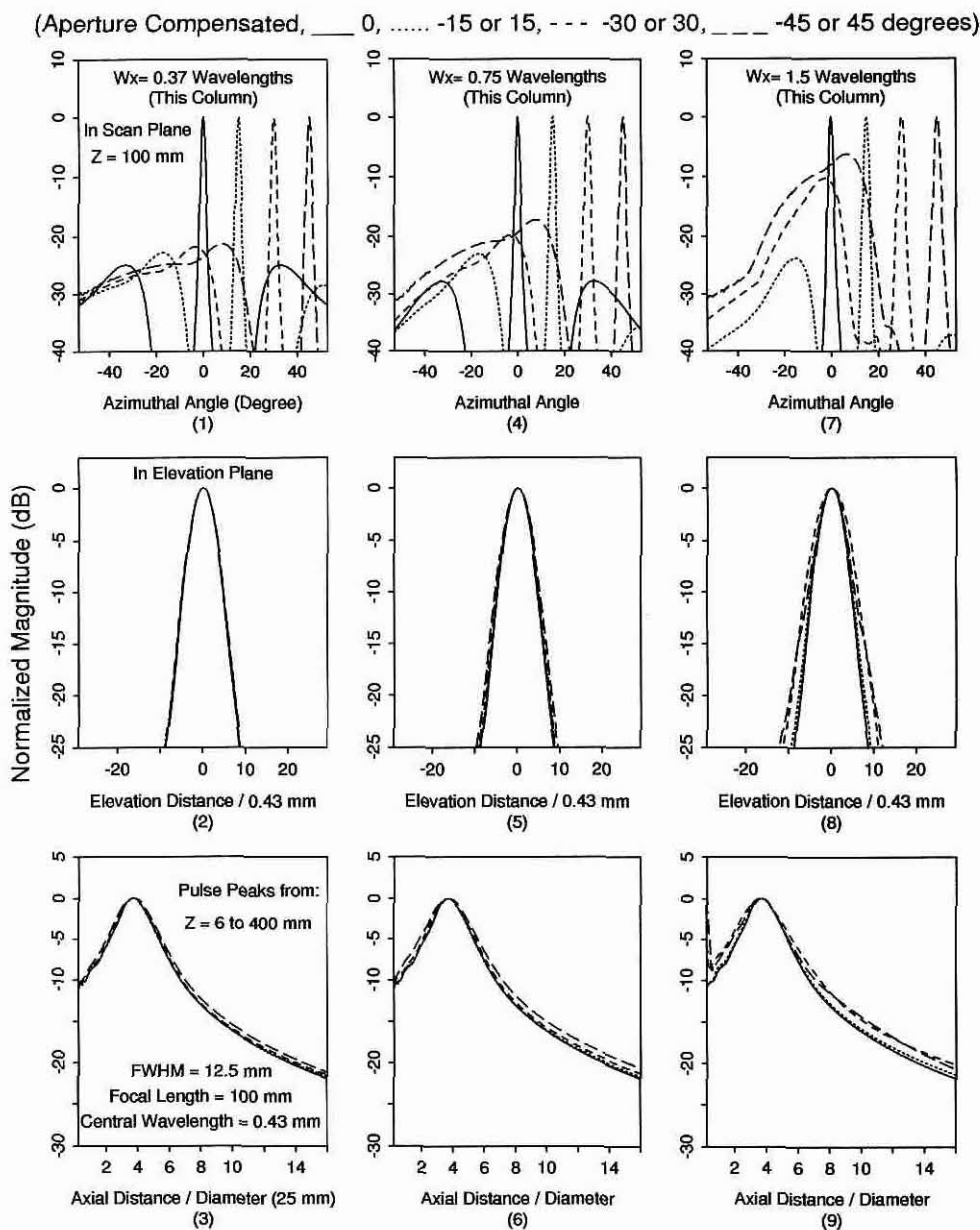


Fig. 10. Comparison of a one-way focused Gaussian beam (the focal length is 100 mm and the FWHM is 12.5 mm at the transducer aperture in the elevation direction) produced with a 2-D array transducer when the widths of the array elements in the scan direction are about 0.37λ (panels in the left column), 0.75λ (panels in the middle column), and 1.5λ (panels in the right column). This figure has the same format and is obtained under the same array conditions as those of Fig. 8.

because the capacitances of the elements may be much smaller than those of the connecting wires. Apparently, for a given interelement distance, reducing the size of elements will lower the energy efficiency of arrays because only a part of the array aperture is used. Therefore, one may want to choose a larger element size while still maintaining a reasonable array performance in a preset range of steering angles (usually in medical imaging, the steering angles are within $\pm 45^\circ$). For the example given in Figs. 8 to 10, the best compromise might be to choose the size of elements in the scan direction as 0.75λ .

D. Reducing System Complexity

To compensate the effective aperture reduction of a 2-D array, the elliptic ring pattern formed by the array elements

must be changed each time a beam is steered to a new direction. In medical imaging, there are typically over 100 directions in a $\pm 45^\circ$ range. This implies that there must be a complicated real-time multiplexing to change the ring patterns that are formed by a large number of elements. However, if the change of the effective aperture is within $\pm 5\%$, beam distortions are not severe (see Figs. 2 to 4, where a $\pm 15^\circ$ steering angle corresponds to an effective aperture reduction of about 3.5%). Because in a $\pm 45^\circ$ range of the steering angles the total change of the effective aperture is about 40%, only 4 elliptic ring patterns are necessary to cover this change. The four elliptic ring patterns may be designed so that they compensate exactly the effective aperture reduction at the following 4 steering angles: $\pm 18^\circ$,

TABLE I
 NORMALIZED MAGNITUDE OF THE PEAK OF BEAMS AND ITS CHANGE WITH THE STEERING ANGLES AND THE ELEMENT SIZES IN THE SCAN DIRECTION. THE INTERELEMENT DISTANCES IN BOTH THE SCAN AND ELEVATION DIRECTIONS ARE THE SAME ($d_{x_1} = d_{y_1}$) AND ARE ABOUT 1.5λ . THE PEAKS OF BEAMS ARE NORMALIZED TO THAT BEFORE THE STEERING.

	Steering Angle (Degree)	Magnitude of Peak (When $w_{y_1} = 0\lambda$ and $w_{x_1} = 0\lambda$) (dB)	Magnitude of Peak (When $w_{y_1} \approx 1.5\lambda$ and $w_{x_1} \approx 0.37\lambda$) (dB)	Magnitude of Peak (When $w_{y_1} \approx 1.5\lambda$ and $w_{x_1} \approx 0.75\lambda$) (dB)	Magnitude of Peak (When $w_{y_1} \approx 1.5\lambda$ and $w_{x_1} \approx 1.5\lambda$) (dB)
Zeroth-Order Bessel Beam	0	0.00	0.00	0.00	0.00
	15	-0.22	-0.37	-0.84	-2.92
	30	-0.07	-0.69	-2.62	-10.8
	45	-0.07	-1.33	-5.33	-17.0
Zeroth-Order X Wave	0	0.00	0.00	0.00	0.00
	15	-0.15	-0.26	-0.67	-2.16
	30	-0.19	-0.67	-2.08	-8.18
	45	-0.18	-1.10	-4.06	-14.2
Focused Gaussian Beam (F = 100 mm)	0	0.00	0.00	0.00	0.00
	15	-0.14	-0.32	-0.85	-2.94
	30	-0.10	-0.74	-2.73	-12.2
	45	-0.05	-1.34	-5.57	-16.8

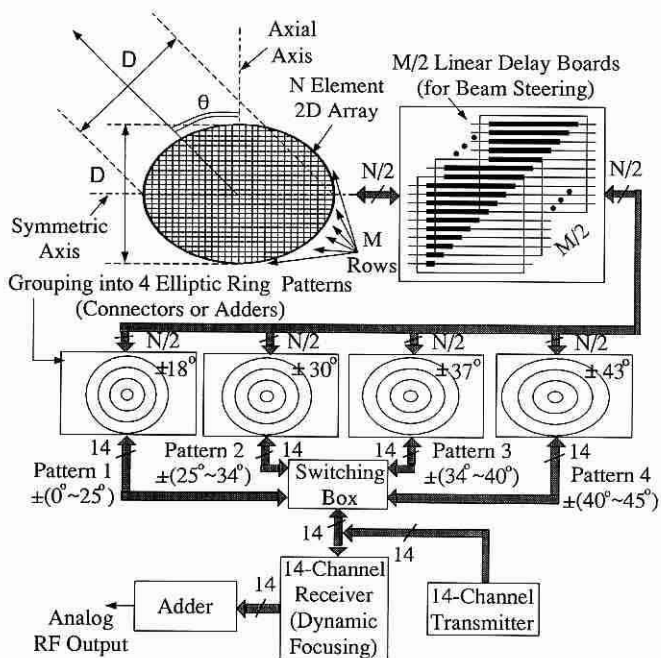


Fig. 11. A schematic of a pulse-echo imaging system using a 2-D array for steering both limited diffraction beams and conventional beams. (Modified with permission from Fig. 5 of [62]).

$\pm 30^\circ$, $\pm 37^\circ$, and $\pm 43^\circ$, and cover the ranges of the steering angles that correspond to the change of the effective aperture within $\pm 5\%$: $\pm(0^\circ \sim 25^\circ)$, $\pm(25^\circ \sim 34^\circ)$, $\pm(34^\circ \sim 40^\circ)$, and $\pm(40^\circ \sim 45^\circ)$ (Fig. 11). Another effective way to simplify the system might be the use of unsymmetrical limited diffraction beams [36]. Instead of changing a ring pattern, one might produce different unsymmetrical limited diffraction beams with the same annular ring pattern as the beams are steered. Similarly, the steering angle can be divided into the above four ranges in which four different unsymmetrical beams are used to reduce the system complexity. In this way, the system

might be simpler because the multiplexing is for the different unsymmetrical limited diffraction beams that are produced with a small number of waveforms (14 in the above example), instead of for different elliptic ring patterns that are formed by a large number of elements.

A suggested pulse-echo imaging system using a 2-D array for steering both limited diffraction beams and conventional beams is shown in Fig. 11 [62]. The array is consist of M rows and has N elements. If beams are symmetric about the scan plane, the number of wires connected out of the array is only $N/2$ (the elements of the lower and upper portions of the array are connected correspondingly inside the array). The $N/2$ wires are connected to $M/2$ linear time delay boards for beam steering. The number of delay elements in each board is equal to the number of the elements in a row. After the linear delays, the $N/2$ wires are grouped electronically into four elliptic patterns each of which covers about $\pm 5\%$ change of the effective aperture. In transmission, a 14 channel transmitter generates 14 waveforms that are multiplexed to drive an elliptic ring pattern selected according to the steering angle of the beams. In reception, echoes delayed with the linear delay boards will be combined into the same elliptic ring pattern, and then processed by a conventional dynamically focused reception circuitry. The system in Fig. 11 is different from a conventional annular array system by adding linear delays and grouping the elements of 2-D arrays into elliptic ring patterns. Because the largest elliptic ring pattern is designed for the compensation of the effective aperture reduction at $\pm 43^\circ$, instead of $\pm 45^\circ$, the number of elements may be reduced slightly.

V. CONCLUSION

Limited diffraction beams can be steered electronically with a 2-D array if the effective aperture reduction of the array is properly compensated. This increases the flexibility of the beams in volumetric imaging and reduces artifacts in real-time color Doppler imaging at the expense of system complexity [18]. The interelement distance of a 2-D array has a significant influence on both limited diffraction beams and conventional beams [46]. For limited diffraction beams with a small main beamwidth, the interelement distance may have to be small to ensure an adequate spatial sampling rate. However, small interelement distance increases the number of array elements dramatically, which complicates array construction. The size of array elements has influence on both limited diffraction beams and conventional beams [46]. Larger element size increases the energy efficiency of arrays and reduces element impedance, but degrades array performance at larger steering angles by increasing grating lobes, lowering gain, and distorting beam shapes.

To produce rotary symmetric limited diffraction beams, elements of a 2-D array must be grouped into elliptic rings such that the projection of the elliptic rings on a plane perpendicular to the beam axis is a constant annular ring pattern. With this annular ring pattern, methods for producing limited diffraction beams or conventional aperture-weighted beams with annular arrays can be applied. If the small change

(a few percents) of the effective aperture is allowed, the number of elliptic ring patterns can be reduced for a complete scan and thus the electronic circuitry can be simplified.

Reduction of the number of the elements of 2-D arrays are desirable. Techniques such as sparse arrays [46] or random position arrays with a minimum interelement distance constraint might be used. However, the influences of these techniques on limited diffraction beams need to be studied.

ACKNOWLEDGMENT

The authors thank Dr. H. Zou for reviewing the manuscript and comments from other three reviewers. The secretarial assistance of E. C. Quarve is appreciated.

REFERENCES

- [1] J. Durnin, "Exact solutions for nondiffracting beams. I. The scalar theory," *J. Opt. Soc. Amer.*, vol. 4, no. 4, pp. 651–654, 1987.
- [2] J. Lu and J. F. Greenleaf, "Nondiffracting X waves—exact solutions to free-space scalar wave equation and their finite aperture realizations," *IEEE Trans. Ultrason., Ferroelec., Freq. Contr.*, vol. 39, no. 1, pp. 19–31, Jan. 1992.
- [3] ———, "Experimental verification of nondiffracting X waves," *IEEE Trans. Ultrason., Ferroelec., Freq. Contr.*, vol. 39, no. 3, pp. 441–446, May 1992.
- [4] ———, "Theory and acoustic experiments of nondiffracting X waves," *IEEE 1991 Ultrason. Symp. Proc.*, 91CH3079–1, vol. 2, pp. 1155–1159, 1991.
- [5] H. Zou, J. Lu, and J. F. Greenleaf, "Obtaining limited diffraction beams with the wavelet transform," *IEEE 1993 Ultrason. Symp. Proc.* 93CH3301–9, vol. 2, pp. 1087–1090, 1993.
- [6] T. K. Song, J. Lu, and J. F. Greenleaf, "Modified X waves with improved field properties," *Ultrason. Imag.*, vol. 15, no. 1, pp. 36–47, Jan., 1993.
- [7] J. Durnin, J. J. Miceli, Jr., and J. H. Eberly, "Diffraction-free beams," *Phys. Rev. Lett.*, vol. 58, no. 15, pp. 1499–1501, Apr. 1987.
- [8] J. Lu, T. K. Song, R. R. Kinnick, and J. F. Greenleaf, "In vitro and in vivo real-time imaging with ultrasonic limited diffraction beams," *IEEE Trans. Med. Imag.*, vol. 12, no. 4, pp. 819–829, Dec. 1993.
- [9] J. Lu and J. F. Greenleaf, "Diffraction-limited beams and their applications for ultrasonic imaging and tissue characterization," in *New Developments in Ultrasonic Transducers and Transducer Systems*, F. L. Lizzi, Ed., *Proc. SPIE*, vol. 1733, pp. 92–119, 1992.
- [10] ———, "Pulse-echo imaging using a nondiffracting beam transducer," *Ultrason. Med. Biol.*, vol. 17, no. 3, pp. 265–281, May, 1991.
- [11] ———, "Ultrasonic nondiffracting transducer for medical imaging," *IEEE Trans. Ultrason., Ferroelec., Freq. Contr.*, vol. 37, no. 5, pp. 438–447, Sept. 1990.
- [12] ———, "Formation and propagation of limited diffraction beams," in *Acoust. Imag.*, vol. 20, Y. Wei and B. Gu, Eds., 1993, pp. 331–343.
- [13] ———, "Effect on J_0 nondiffracting beam of deleting central elements of J_0 annular array transducer," *Ultrason. Imag.*, vol. 13, no. 2, p. 203, Apr. 1991 (Abs).
- [14] ———, "Experiment of imaging contrast of J_0 Bessel nondiffracting beam transducer," *J. Ultrasound Med.*, vol. 11, no. 3, (Suppl.), p. S43, Mar. 1992 (Abs).
- [15] ———, "Simulation of imaging contrast of nondiffracting beam transducer," *J. Ultrasound Med.*, vol. 10, no. 3, (Suppl.), p. S4, Mar., 1991 (Abs).
- [16] D. K. Hsu, F. J. Margetan, and D. O. Thompson, "Bessel beam ultrasonic transducer: Fabrication method and experimental results," *Appl. Phys. Lett.*, vol. 55, no. 20, pp. 2066–2068, Nov. 1989.
- [17] J. A. Campbell and S. Soloway, "Generation of a nondiffracting beam with frequency independent beam width," *J. Acoust. Soc. Amer.*, vol. 88, no. 5, pp. 2467–2477, Nov. 1990.
- [18] P. A. Magnin, "A review of Doppler flow mapping techniques," *IEEE 1987 Ultrason. Symp. Proc.*, 87CH2492–7, vol. 2, pp. 969–977, 1987.
- [19] J. Lu and J. F. Greenleaf, "Evaluation of a nondiffracting transducer for tissue characterization," *IEEE 1990 Ultrason. Symp. Proc.*, 90CH2938–9, vol. 2, pp. 795–798, 1990.
- [20] ———, "Producing deep depth of field and depth-independent resolution in NDE with limited diffraction beams," *Ultrason. Imag.*, vol. 15, no. 2, pp. 134–149, Apr., 1993.
- [21] J. N. Brittingham, "Focus wave modes in homogeneous Maxwell's equations: transverse electric mode," *J. Appl. Phys.*, vol. 54, no. 3, pp. 1179–1189, 1983.
- [22] R. W. Ziolkowski, "Exact solutions of the wave equation with complex source locations," *J. Math. Phys.*, vol. 26, no. 4, pp. 861–863, Apr., 1985.
- [23] R. W. Ziolkowski, D. K. Lewis, and B. D. Cook, "Evidence of localized wave transmission," *Phys. Rev. Lett.*, vol. 62, no. 2, pp. 147–150, Jan. 9, 1989.
- [24] R. W. Ziolkowski, "Localized transmission of electromagnetic energy," *Phys. Rev. A*, vol. 39, no. 4, pp. 2005–2033, Feb. 15, 1989.
- [25] R. Donnelly, D. Power, G. Templeman, and A. Whalen, "Graphic simulation of superluminal acoustic localized wave pulses," *IEEE Trans. Ultrason., Ferroelec., Freq. Contr.*, vol. 41, no. 1, pp. 7–12, 1994.
- [26] R. Donnelly and R. W. Ziolkowski, "Designing localized waves," *Proc. Royal Soc. Lond., A*, vol. 440, pp. 541–565, 1993.
- [27] K. Uehara and H. Kikuchi, "Generation of near diffraction-free laser beams," *Appl. Phys. B*, vol. 48, pp. 125–129, 1989.
- [28] A. Vasara, J. Turunen, and A. T. Friberg, "Realization of general nondiffracting beams with computer-generated holograms," *J. Opt. Soc. Amer. A*, vol. 6, no. 11, pp. 1748–1754, 1989.
- [29] G. Indebetow, "Nondiffracting optical fields: some remarks on their analysis and synthesis," *J. Opt. Soc. Amer. A*, vol. 6, no. 1, pp. 150–152, Jan., 1989.
- [30] F. Gori, G. Guattari, and C. Padovani, "Model expansion for J_0 -correlated Schell-model sources," *Optics Commun.*, vol. 64, no. 4, pp. 311–316, Nov. 15, 1987.
- [31] F. Gori, G. Guattari, and C. Padovani, "Bessel-Gaussian beams," *Optics Commun.*, vol. 64, no. 6, pp. 491–495, Dec. 15, 1987.
- [32] K. Uehara and H. Kikuchi, "Generation of near diffraction-free laser beams," *Appl. Phys. B*, vol. 48, pp. 125–129, 1989.
- [33] L. Vicari, "Truncation of nondiffracting beams," *Optics Commun.*, vol. 70, no. 4, pp. 263–266, Mar. 1989.
- [34] M. Zahid and M. S. Zubairy, "Directionally of partially coherent Bessel-Gauss beams," *Optics Commun.*, vol. 70, no. 5, pp. 361–364, Apr. 1989.
- [35] S. Y. Cai, A. Bhattacharjee, and T. C. Marshall, "'Diffraction-free' optical beams in inverse free electron laser acceleration," *Nuclear Instrum. and Methods in Physics Res., Section A: Accelerators, Spectrometers, Detectors, and Associated Equip.*, vol. 272, no. 1–2, pp. 481–484, Oct., 1988.
- [36] J. Lu, H. Zou, and J. F. Greenleaf, "Biomedical ultrasound beam forming," *Ultrason. Med. Biol.* vol. 20, no. 5, pp. 403–427, 1994.
- [37] F. S. Foster, M. S. Patterson, M. Arditi, and J. W. Hunt, "The conical scanner: A two transducer ultrasound scatter imaging technique," *Ultrason. Imag.*, vol. 3, no. 1, pp. 62–82, 1981.
- [38] D. R. Dietz, "Apodized conical focusing for ultrasound imaging," *IEEE Trans. Sonics Ultrason.*, vol. SU-29, no. 3, pp. 128–138, May 1982.
- [39] M. O'Donnell, "A proposed annular array imaging system for contact B-scan applications," *IEEE Trans. Sonics Ultrason.*, vol. SU-29, no. 6, pp. 331–338, Nov. 1982.
- [40] E. K. Fishell, F. S. Foster, T. Connor, M. Khodai, K. Harasciewicz, and J. W. Hunt, "Clinical performance of a cone / annular array ultrasound breast scanner," *Ultrason. Med. Biol.*, vol. 16, no. 4, pp. 361–374, Nov. 1990.
- [41] F. S. Foster and J. W. Hunt, "The focusing of ultrasound beams through human tissue," in *Acoust. Imag.*, vol. 8, pp. 709–718, 1979.
- [42] G. E. Trahey, P. D. Freiburger, L. F. Nock, and D. C. Sullivan, "In vivo measurements of ultrasonic beam distortion in the breast," *Ultrason. Imag.*, vol. 13, no. 1, pp. 71–90, 1991.
- [43] F. S. Foster, J. D. Larson, M. K. Mason, T. S. Shoup, G. Nelson, and H. Yoshida, "Development of a 12 element annular array transducer for realtime ultrasound imaging," *Ultrason. Med. Biol.*, vol. 15, no. 7, pp. 649–659, 1989.
- [44] F. S. Foster, J. D. Larson, R. J. Pittaro, P. D. Corl, A. P. Greenstein, and P. K. Lum, "A digital annular array prototype scanner for realtime ultrasound imaging," *Ultrason. Med. Biol.*, vol. 15, no. 7, pp. 661–672, 1989.
- [45] O. T. Von Ramm and S. W. Smith, "Beam steering with linear arrays," *IEEE Trans. Biomed. Imag.*, vol. BME-30, pp. 438–452, 1983.
- [46] D. H. Turnbull and F. S. Foster, "Beam steering with pulsed 2-D transducer arrays," *IEEE Trans. Ultrason., Ferroelec., Freq. Contr.*, vol. 38, no. 4, pp. 320–333, July 1991.
- [47] D. H. Turnbull and F. S. Foster, "Fabrication and characterization of transducer elements in 2-D arrays for medical ultrasound imaging," *IEEE Trans. Ultrason., Ferroelec., Freq. Contr.*, vol. 39, no. 4, pp. 464–475, Jul. 1992.
- [48] S. W. Smith, H. E. Pavy, Jr., and O. T. von Ramm, "High-speed ultrasound volumetric imaging system—Part I: Transducer design and

- beam steering," *IEEE Trans. Ultrason., Ferroelec., Freq. Contr.*, vol. 38, no. 2, pp. 100–108, Mar., 1991.
- [49] L. F. Nock and G. E. Trahey, "Synthetic receive aperture imaging with phase correction for motion and for tissue inhomogeneities — Part I: Basic Principles," *IEEE Trans. Ultrason., Ferroelec., Freq. Contr.*, vol. 39, no. 4, pp. 489–495, Jul. 1992.
- [50] G. S. Kino, *Acoustic waves: Devices, Imaging, and Analog Signal Processing*. Englewood Cliffs, NJ: Prentice-Hall, 1987, ch. 2 and 3.
- [51] F. John, *Partial Differential Equations*. New York: Springer-Verlag, 1982.
- [52] P. M. Morse and H. Feshbach, *Methods of Theoretical Physics*, Part I. New York: McGraw-Hill, 1953.
- [53] I. S. Gradshteyn and I. M. Ryzhik, *Table of Integrals, Series, and Products*, corrected and enlarged edition. New York: Academic, 1980, ch. 17.
- [54] J. Lu and J. F. Greenleaf, "Sidelobe reduction for limited diffraction pulse-echo systems," *IEEE Trans. Ultrason., Ferroelec., Freq. Contr.*, vol. 40, no. 6, pp. 735–746, Nov. 1993.
- [55] J. W. Goodman, *Introduction to Fourier Optics*. New York, NY: McGraw-Hill, 1968, ch. 2–4.
- [56] R. Bracewell, *The Fourier transform and its Applications*. New York: McGraw-Hill, 1965, ch. 4 and 6.
- [57] A. V. Oppenheim and R. W. Schaffer, *Digital Signal Processing*. Englewood Cliffs, NJ: Prentice-Hall, 1975, ch. 1 and 5.
- [58] B. D. Steinberg, *Principles of Aperture and Array System Design*. New York: Wiley, 1976.
- [59] J. Lu and J. F. Greenleaf, "A study of sidelobe reduction for limited diffraction beams," *IEEE 1993 Ultrason. Symp. Proc.* 93CH3301–9, vol. 2, pp. 1077–1082, 1993.
- [60] ———, "Sidelobe reduction of nondiffracting pulse-echo images by deconvolution," *Ultrason. Imag.*, vol. 14, no. 2, p. 203, Apr. 1992 (Abs).
- [61] A. Rosenfeld and A. C. Kak, *Digital Picture Processing*. New York: Academic, 2nd ed., vol. 1, 1982, ch. 7.
- [62] J. Lu and J. F. Greenleaf, "Steering of limited diffraction beams with a 2-D array transducer," *IEEE 1992 Ultrason. Symp. Proc.*, 92CH3118–7, vol. 1, pp. 603–607, 1992.
- [63] R. L. Goldberg and S. W. Smith, "Performance of multi-layer 2-D transducer arrays," *IEEE 1993 Ultrason. Symp. Proc.*, 93CH3301–9, vol. 2, pp. 1103–1106, 1993.

Jian-yu Lu (M'88), for a photograph and biography, see p. 424 of the July 1994 issue of this TRANSACTIONS.

James F. Greenleaf (M'73–SM'84–F'88), for a photograph and biography, see p. 424 of the July 1994 issue of this TRANSACTIONS.